Linking elementary-fibre/lumen size gradients to multi-view micro-DIC strain localization and fracture modes in technical bamboo fibres

C. Cardona[1,2], L. Garcia-Palacio[1,3] and C.A. Fuentes[1,4]*

[1] Structural Composites Unit, Luxembourg Institute of Science and Technology (LIST), Luxembourg, Luxembourg

[2] Department of Physics and Materials Science, University of Luxembourg, Luxembourg, Luxembourg

[3]Universidad Autónoma de Manizales, Departamento de Electrónica y Automatización, Manizales, Colombia

[4] Department of Materials Engineering, KU Leuven, Leuven, Belgium*

Corresponding author: carlos.fuentes@list.lu

Keywords: *Bamboo fibre; Deep learning segmentation; Micro-DIC; Photogrammetry; Damage mechanisms*

1. Abstract

Technical bamboo fibres exhibit a strongly heterogeneous, hierarchical architecture in which tubular elementary fibres with central lumens are bonded by a lignin-rich middle lamella, leading to large scatter in tensile response and fracture modes. This work quantifies how microstructural design parameters—phase fractions, spatial arrangement and growth-related expansion gradients—govern tensile strain localization and failure mechanisms, enabling microstructure-informed fibre selection and bio-inspired composite design for composites.

Advanced multimodal characterization was performed at the technical-fibre and microstructural scales. Single-fibre tensile tests (gauge length 20 mm; cross-head speed 0.2 mm/min) yielded a tensile strength of 585 ± 51 MPa, failure strain of 1.67 ± 0.17%, and Young's modulus of 35.15 ± 3.83 GPa. To link these macroscopic metrics to internal architecture, cross-section images and micro-CT were analysed using a deep-learning segmentation workflow based on RootPainter, achieving IoU = 0.817 and Dice = 0.900 on bamboo fibre images. The segmented phase fractions were quantified as 0.096 (lumens), 0.155 (middle lamella) and 0.7489 (elementary fibres), enabling spatial statistics of void/matrix distributions and comparison with micro-CT-derived density patterns.

In-situ microscale deformation was resolved by micro-digital image correlation (micro-DIC), supported by photogrammetry for damage/fracture-shape digitalization, producing full-field strain maps (ε_{xx}, εyy, εxy) over multiple loading increments. The strain fields reveal oscillatory and strongly localized patterns that correlate with (i) local elementary-fibre packing/arrangement and (ii) cross-sectional gradients in lumen and elementary-fibre size distribution, providing mechanistically grounded indicators of crack initiation. Three characteristic fracture morphologies

were identified and interpreted from the combined microstructural, micro-DIC, and photogrammetry data. Semi-clean fractures were associated with more ordered spatial configurations and higher apparent bundle-level cooperation, consistent with improved stress redistribution pathways.

2. Introduction

Plant-based technical fibres such as bamboo combine high specific stiffness and strength with significant sustainability potential for composite materials. In contrast to synthetic fibres with nearly uniform cylindrical geometry, bamboo technical fibres consist of bundles of tubular elementary fibres with central lumens bonded by a lignin-rich middle lamella, producing a complex multiphase architecture with polygonal cell-wall geometries and pronounced heterogeneity across the cross-section. A representative transverse cross-section highlighting lumens, elementary fibres and middle lamella is shown in **Figure 1**, illustrating the strong variability in lumen shape and size as well as in cell-wall thickness within a single technical fibre.

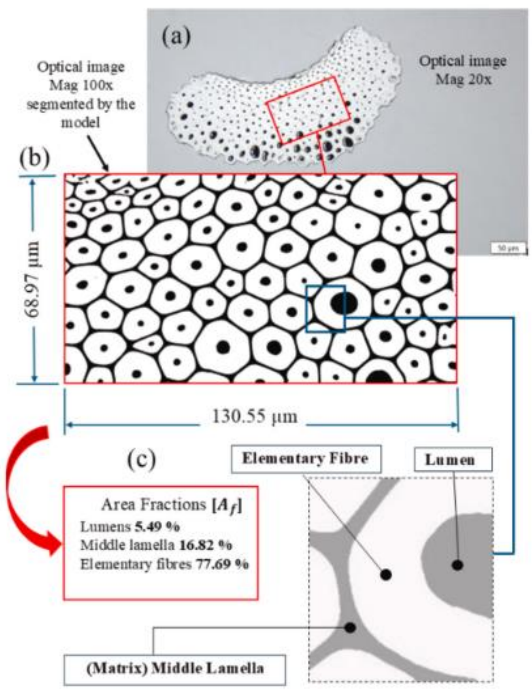

Figure 1. Representative transverse cross-section of a technical bamboo fibre showing lumens, elementary fibres, and middle lamella.

Although tensile strength and Young's modulus of single bamboo fibres have been widely reported, phase-resolved quantification of cross-sectional geometric features—such as lumen size, middle-lamella thickness and elementary-fibre wall area—remains limited, restricting detailed structure–property analysis and micromechanical modelling. Previous studies on bamboo have demonstrated that radial variations in vascular-bundle distribution and fibre volume fraction strongly influence stiffness and strength, while recent work has linked graded distributions of bundle area and density to tensile and flexural response in different bamboo species. Analogous micro-tomography-based studies on flax show that accurate description of defects and local heterogeneity is essential for reliable prediction of natural-fibre mechanical behaviour, further emphasising the need for quantitative microstructural descriptors in bamboo.

Traditional image analysis pipelines for natural fibres rely mainly on grayscale thresholding and clustering applied to optical or micro-CT data. While computationally inexpensive, these methods are sensitive to noise and local contrast, often causing incorrect void splitting, edge smoothing and mis-classification of phases that propagate directly into morphological descriptors used as input for micromechanical models. Conventional laboratory micro-CT at voxel sizes of about 0.7–1.4 µm struggles to resolve sub-micron intercellular layers such as the middle lamella, which play a central role in inter-fibre bonding and load transfer in natural-fibre composites. As a result, many analyses effectively collapse the three-phase architecture into only two phases, limiting insight into interfacial mechanisms.

Deep-learning-based segmentation has recently emerged as a promising route to overcome these limitations by providing accurate, automated, phase-resolved maps of natural-fibre microstructure. In earlier work, we developed a RootPainter-based segmentation framework for bamboo technical fibre cross-sections, achieving high Dice and IoU scores while requiring only moderate annotation effort. The segmentation pipeline, together with subsequent ImageJ-based morphometric analysis and web-based visualisation, is summarised schematically in **Figure 2**. That study showed that deep learning enables reliable separation of lumen, elementary fibres and middle lamella, and supports advanced descriptors such as kernel-density maps and gradient-field representations of lumen and cell-wall areas.

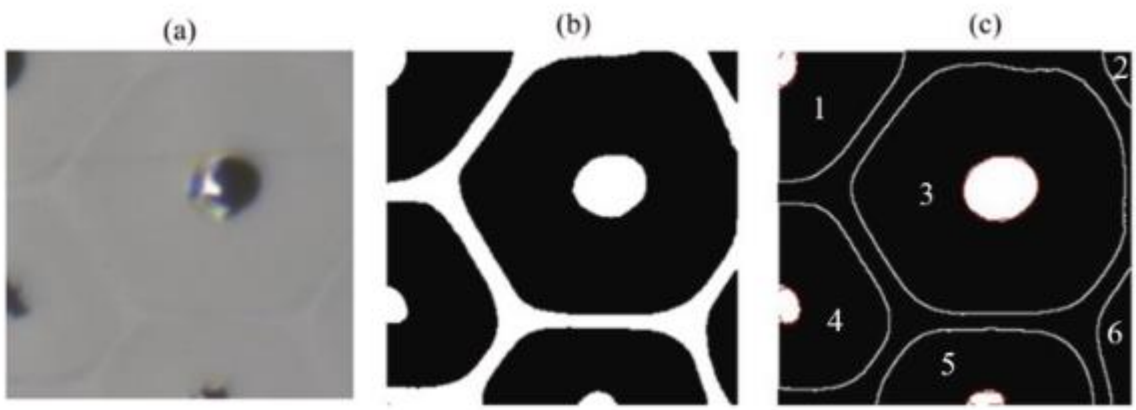

Figure 2. Schematic of the deep-learning segmentation and morphometric analysis workflow used to quantify bamboo fibre microstructure.

However, a direct link between such microstructural descriptors and the tensile strain localisation and fracture mechanisms of technical bamboo fibres has not yet been demonstrated. The objective of the present work is therefore to combine deep-learning-based microstructural analysis, 3D shape characterisation and multi-view micro-digital image correlation (micro-DIC) to quantify how elementary-fibre and lumen gradients govern strain localisation and fracture morphology in single technical fibres. A representative 3D reconstruction of a technical fibre, together with axial strain fields obtained by micro-DIC at increasing load levels, is presented in **Figure 3** and forms the backbone of the multimodal analysis developed in this paper.

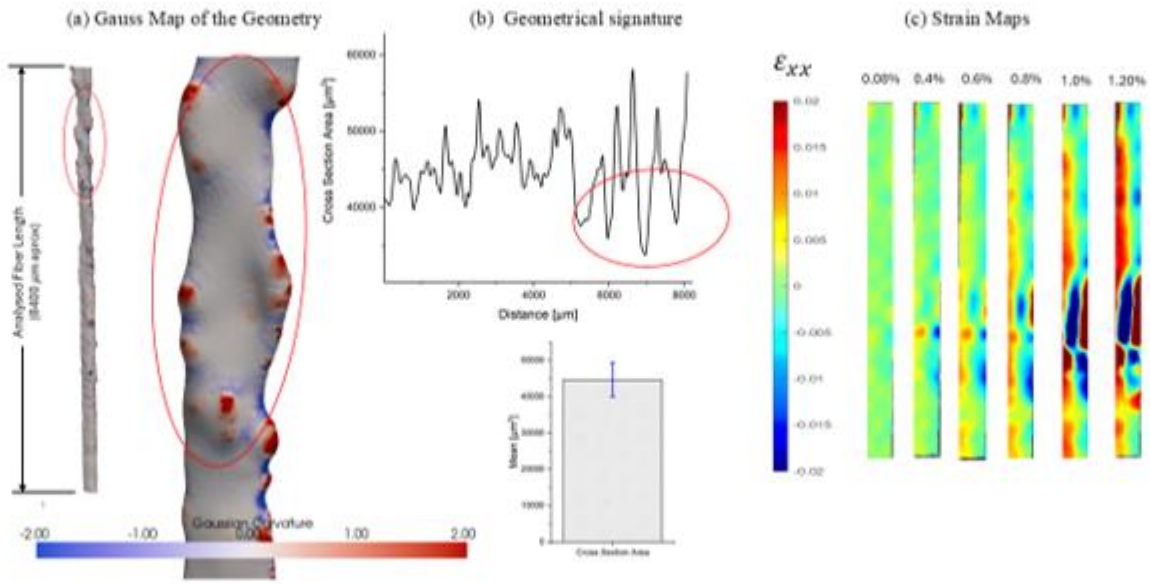

Figure 3. Multimodal characterisation of a technical bamboo fibre, including 3D reconstruction and micro-DIC strain fields at increasing load levels.

3. Experimental methods

3.1. Materials and mechanical testing

Technical bamboo fibres from *Guadua angustifolia* were extracted mechanically from culms harvested in a tropical plantation near Manizales, Colombia, avoiding chemical treatments that could modify cell-wall properties. Individual technical fibres were carefully separated, inspected to avoid visible defects, and conditioned at laboratory environment prior to testing. Quasi-static tensile tests were performed on single technical fibres with a nominal gauge length of 20 mm at a cross-head speed of 0.2 mm/min using paper tab grips to minimise slippage and premature grip damage. Engineering stress–strain curves yielded average tensile strength of 585 ± 51 MPa, failure strain of 1.67 ± 0.17%, and Young's modulus of 35.15 ± 3.83 GPa, in line with values reported for high-quality bamboo technical fibres.

3.2. Microstructural imaging and deep-learning segmentation

For cross-sectional microstructural analysis, technical fibres from the same batch were embedded in cold-mounting epoxy, ultramicrotomed perpendicular to the fibre axis with a pitch down to 250 nm, and imaged at 20× and 100× magnification using an optical microscope. A representative transverse micrograph at 20× magnification, highlighting the lumen, elementary-fibre and middle-lamella phases, is shown in **Figure 1**, together with a schematic indication of the anatomical regions used in the analysis. High-resolution micrographs (2052 × 1086 px) acquired at 100× magnification were cropped into patches to build a dataset for deep-learning segmentation.

The segmentation process followed the RootPainter-based workflow previously established for bamboo fibres, as summarised in **Figure 4**. Briefly, cropped images were annotated in RootPainter using lumen and middle lamella as foreground and elementary fibres as background, following a technical convention that simplifies subsequent processing. The final RootPainter model, based on a U-Net-derived architecture with residual blocks and group normalisation, was trained on 1 025 images and tested on 205 images, achieving validation Dice and IoU scores of approximately 0.91 and 0.83, respectively. For the present study, this model was applied to cross-section images corresponding to the mechanically tested fibres, generating binary masks for the three anatomical phases.

Morphological metrics—areas, perimeters, centroids, and ellipse-fit parameters—were computed in ImageJ from the segmented masks, following the workflow summarised in **Figure 4**. A circularity threshold of 0.4 was used to distinguish lumens from the other phases, and phase area fractions were calculated by combining lumen masks with the total segmented fibre area, assigning remaining pixels to elementary fibres and middle lamella. Spatial statistics, including kernel-density maps and gradient-field descriptors of lumen and elementary-fibre areas, were derived from these masks; representative examples are presented in **Figure 6**.

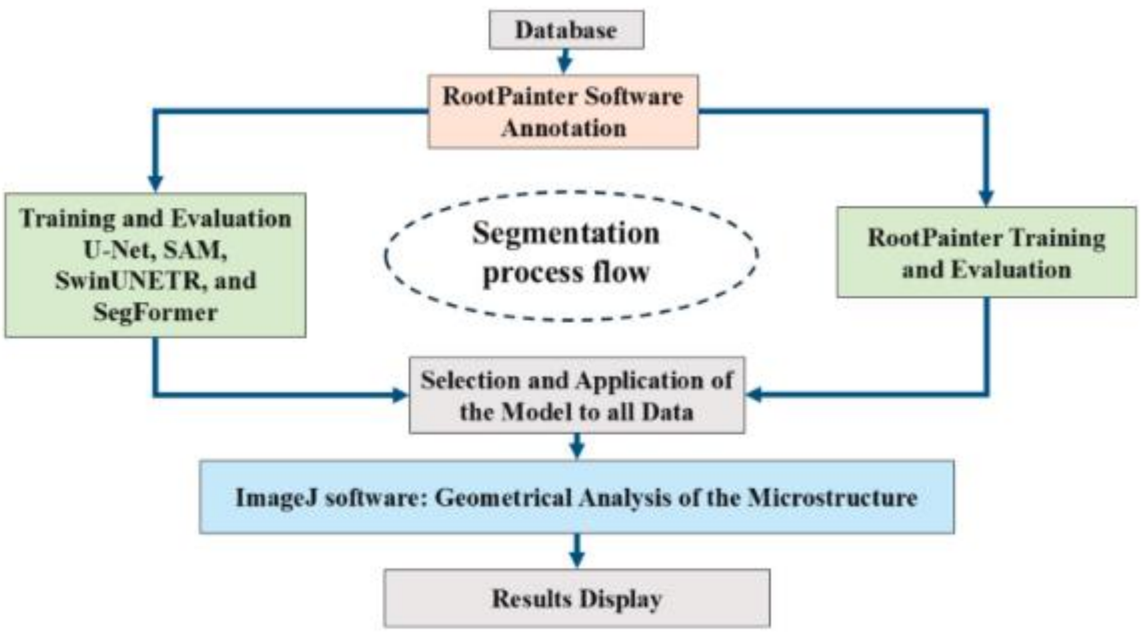

Figure 4. RootPainter-based segmentation workflow and downstream ImageJ morphometric analysis for bamboo fibre cross-sections.

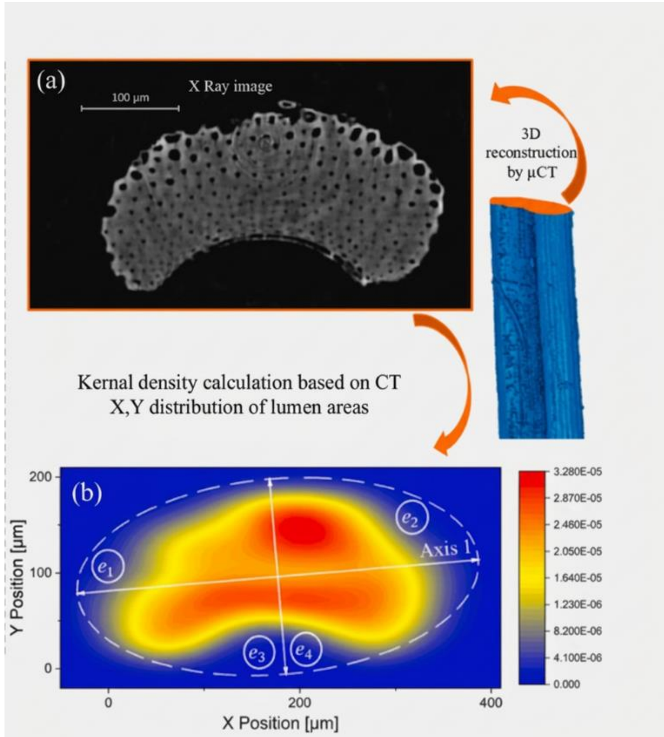

Figure 5. Microstructural spatial descriptors of bamboo fibre cross-sections, including kernel-density mapping of lumen centroids and gradient-field analysis of lumen and elementary-fibre areas.

3.3. Micro-CT and 3D geometry reconstruction

Additional fibres from the same batch were scanned by micro-computed tomography at a voxel size of approximately 1 µm to obtain independent information on lumen distributions and global fibre geometry. The reconstructed volumes were used to generate surface meshes and Gauss-curvature maps of the external fibre shape, as well as to locate lumen centroids and approximate lumen area along the fibre length. A representative 3D reconstruction, together with a Gauss-curvature map of the surface and a longitudinal "geometrical signature" of cross-sectional area variation, is shown in **Figure 3a–b**.

3.4. Micro-DIC and photogrammetry

In-situ microscale deformation was monitored by micro-digital image correlation during tensile loading of technical fibres. A high-magnification optical system recorded images of the fibre surface at multiple load levels, using an appropriate speckle pattern on the fibre or backing to enable reliable correlation. Full-field strain maps ε_{xx}, εyy and εxy were obtained using standard DIC algorithms, delivering spatially resolved strain distributions along the fibre gauge length at successive load steps. Representative axial strain maps at different global strain levels are displayed in **Figure 3c**, where the emergence of localised high-strain bands along the fibre length can be clearly observed.

Photogrammetry was employed to capture the 3D fracture shape and global fibre curvature at failure, allowing the micro-DIC data to be co-registered with the 3D geometry and with the reconstructed micro-CT volume. This multi-view framework enabled direct comparison between local surface strain concentrations, cross-sectional architecture and global shape features such as local tapering or curvature.

4. Results and discussion

4.1. Tensile response and scatter

The single-fibre tensile tests confirmed the high specific stiffness and strength of technical *Guadua* fibres, with average strength, modulus and failure strain consistent with values reported for high-quality bamboo technical fibres and other high-performance natural fibres. Stress–strain curves exhibited an initially linear response up to about 1% strain, followed by slight non-linearity and abrupt load drops associated with local damage events, before final brittle failure. The tensile response exhibited scatter consistent with the underlying heterogeneity in internal architecture and motivates the detailed microstructural and strain-field analysis presented below.

4.2. Phase fractions and microstructural gradients

Deep-learning segmentation of the cross-sections yielded phase fractions of 0.096 for lumens, 0.155 for middle lamella and 0.7489 for elementary fibres in the technical fibre considered as reference. These values, extracted from masks such as those illustrated in **Figure 6**, indicate that elementary fibres occupy the majority of the cross-section, with the middle lamella representing a substantial fraction of solid material responsible for inter-fibre bonding. **Figure 6a** shows the mirrored original optical micrograph, while **Figure 6b–c** present the RootPainter segmentation and contour-annotated masks used for quantitative analysis, highlighting the ability of the deep-learning workflow to resolve thin middle-lamella regions that are difficult to capture with conventional thresholding.

Kernel-density maps of lumen centroids, such as the example shown in **Figure 5**, revealed a functionally graded organisation in which large lumens tend to cluster away from the neutral axis, whereas a lumen-poor corridor runs approximately along the geometric centre of the cross-section. Gradient-field maps of lumen and elementary-fibre areas, presented in **Figure 5b**, showed intermittent zones of high geometric change rate, corresponding to regions where lumen expansion or contraction is particularly pronounced over short distances. Together, these descriptors suggest that bamboo optimises bending performance by concentrating solid material near the neutral axis and placing lumen-rich, lightweight regions towards zones of high tensile or compressive stress.

4.3. Strain localisation from micro-DIC

Micro-DIC strain maps, exemplified in **Figure 3c**, displayed oscillatory axial strain patterns along the fibre, with localised bands of high ε_{xx} alternating with lower-strain regions even under nominally uniform tensile loading. When projected onto the 3D geometry and aligned with cross-sectional locations for which deep-learning segmentation was available, these high-strain bands were found to correlate strongly with local variations in lumen content and elementary-fibre wall area indicated by the maps in **Figures 5 and 6**. Regions where the cross-section exhibits larger lumens and thinner elementary-fibre walls tended to develop higher axial strains and shear concentrations, indicating locally reduced stiffness and enhanced stress amplification.

Conversely, zones with tightly packed elementary fibres and small lumens—corresponding to the lumen-poor corridor identified in **Figure 5a**—showed more homogeneous strain fields and delayed localisation, consistent with more effective load sharing among fibres. The combination of deep-learning-based segmentation and micro-DIC therefore reveals that strain localisation is not random but guided by the graded microstructural architecture of the technical fibre.

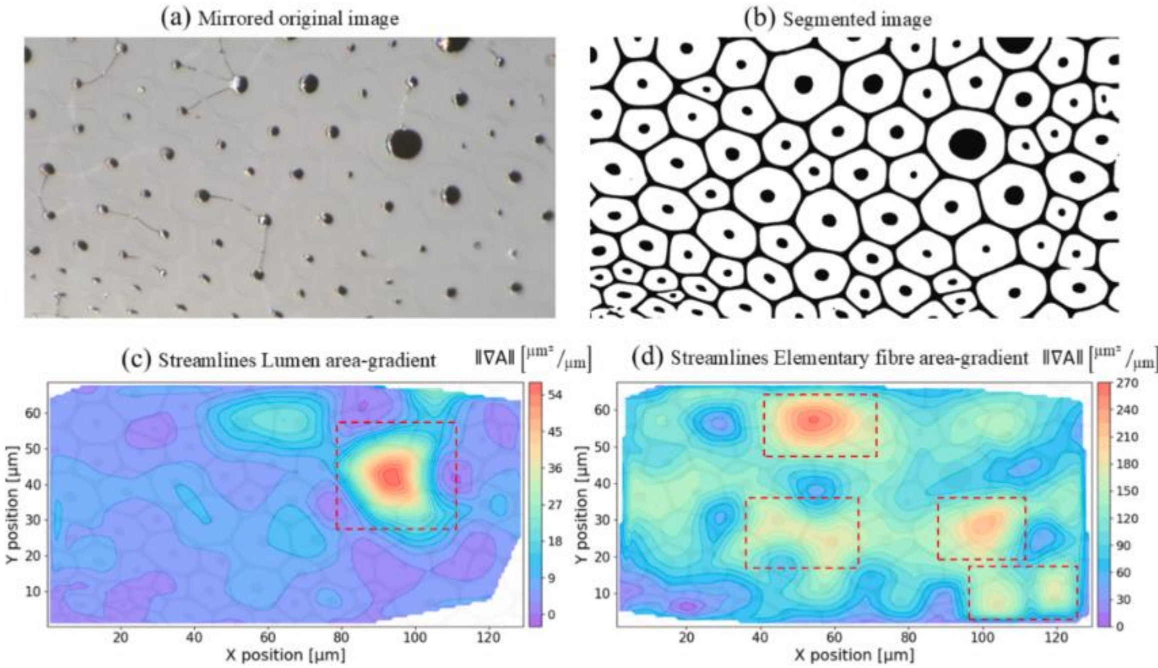

Figure 6. Cross-sectional microstructure, strain localisation, and fracture morphologies of technical bamboo fibres, linking phase architecture to damage modes.

4.4. Fracture morphologies and microstructural control

The three dominant fracture morphologies illustrated in **Figure 6** can now be interpreted in light of the strain and microstructural descriptors. Semi-clean fractures, characterised by relatively planar fracture surfaces with limited fibre pull-out, were typically associated with fibres whose cross-sections showed moderate lumen content, balanced radial distributions and limited extreme gradients in elementary-fibre area, leading to more homogeneous strain fields. Central defibrillation, in which the bundle splits near its centre, occurred preferentially in fibres where large central lumens and weaker middle-lamella bridges coincided with intense axial strain bands identified in **Figure 1c** and with strong local gradients in lumen area highlighted in **Figure 5b**.

Asymmetric defibrillation, featuring preferential splitting on one side of the bundle, was linked to cross-sections with strongly asymmetric lumen or elementary-fibre gradients and to micro-DIC fields showing pronounced shear strain concentrations near one lateral region. These observations support a mechanistic picture in which competing normal-stress-driven cell-wall rupture (governed by elementary-fibre properties) and shear-driven inter-elementary-fibre separation (controlled by middle-lamella geometry and distribution) jointly determine fracture morphology. The figures together show how local architecture, captured quantitatively by deep learning, guides the emergence of these macroscopic failure patterns.

5. Conclusions

In conclusion, this study demonstrates that combining deep-learning-based segmentation, high-resolution microscopy, micro-CT and multi-view micro-DIC provides a powerful framework to connect the heterogeneous microstructure of technical bamboo fibres with their tensile strain localization and fracture behaviour. RootPainter-based segmentation delivered robust three-phase maps of lumen, elementary fibres and middle lamella with high Dice and IoU scores, enabling quantitative phase fractions and spatial descriptors that capture the functionally graded character of the fibre cross-section. The analysed technical fibre exhibited lumen, middle-lamella and elementary-fibre area fractions on the order of 0.096, 0.155 and 0.7489, respectively, while kernel-density and gradient-field analyses revealed lumen-poor corridors and intermittent zones of rapid geometric change that are consistent with bending-optimized architectures in the natural material.

By linking these descriptors to micro-DIC strain maps, we showed that axial and shear strain localization does not occur randomly, but instead follows local variations in lumen content, elementary-fibre wall thickness and cross-sectional geometry, as captured by both optical segmentation and micro-CT-based shape reconstruction. Regions with larger lumens and thinner cell walls developed higher strain concentrations and acted as preferential sites for damage initiation, whereas more uniformly packed elementary-fibre regions sustained more homogeneous strains and delayed localization. The observed fracture morphologies—ranging from semi-clean fracture to central and asymmetric defibrillation—could therefore be interpreted as the macroscopic manifestation of this microstructural landscape, emerging from the competition between normal-stress-driven cell-wall rupture and shear-driven separation along middle-lamella interfaces.

Overall, the results indicate that phase-resolved microstructural metrics, when combined with full-field strain measurements, provide microstructure-informed indicators for technical-fibre selection and offer a route towards bio-inspired composite design strategies that exploit, rather than average out, the intrinsic heterogeneity of bamboo fibres. The methodology developed here is readily transferable to other natural-fibre systems and can serve as an image-based input generator for micromechanical and finite-element models, thereby supporting multi-scale design and reliability assessment of sustainable composite materials

6. References

[1] Amada, S., Ichikawa, Y., Munekata, T., Nagase, Y., & Shimizu, H. (1997). Fiber texture and mechanical graded structure of bamboo. Composites Part B: Engineering, 28(1–2), 13–20.

[2] Dixon, P. G., & Gibson, L. J. (2014). The structure and mechanics of Moso bamboo material. Journal of the Royal Society Interface, 11(99).

[3] Li, H., Zhu, Q., Lu, P., Chen, X., & Xian, Y. (2024). The gradient variation of location distribution, cross-section area, and mechanical properties of Moso bamboo vascular bundles along the radial direction. Forests, 15(6), 1023.

[4] Zhang, K., Yu, L., Dai, F., Chen, Y., Jiang, Z., Wang, Y., & Tian, G. (2024). Bamboo structure and its impact on mechanical properties: A case study of Bambusa arundinacea. Forests, 15(5), 762.

[5] Fakhreddine, Y., Rajakumaran, M., Guessasma, T., et al. (2024). Impact of defects on tensile properties of ancient and modern Egyptian flax fibers: Multiscale X-ray microtomography and numerical modelling. Fibers, 12(12), 111.

[6] Garcia-Palacio, L. M., Cardona, C. I., Alzate-Grisales, J. A., Dieden, R., Delfrari, D., Cardona-Morales, O., Bravo-Ortiz, M. A., & Fuentes, C. A. (2025). Integrating deep learning and geometry-based microstructural analysis of bamboo technical fibers for bio-composite engineering. Composites Part A: Applied Science and Manufacturing, 2026.

[7] Cardona, C. I., Garcia, L. M., & Fuentes, C. A. (2025). Deep learning-based geometrical analysis and tension strain mapping of bamboo fibre microstructure. In Proceedings of the 24th International Conference on Composite Materials (ICCM-24), Baltimore, USA, 4–8 August 2025.